

area for further study.

We would like to thank the operating crew of the Cornell 10-GeV machine for supplying a beam of excellent quality throughout the data-taking phase

of the experiment. R. Helmke performed a major service both with the time-sharing software for the IBM 1800 computer and with an assembly language routine for the magnet integration which considerably improved the analysis time. A. Loomis helped with the early stages of the experiment.

*Work supported by the National Science Foundation.

†Present address: Laboratori Nazionali di Frascati, Italy.

¹A summary of the data up to 1969 along with a phenomenological analysis appears in a paper by R. L. Walker, Phys. Rev. **182**, 1729 (1969).

²G. Fischer *et al.*, paper submitted to the Fifteenth International Conference on High-Energy Physics, Kiev, U.S.S.R., 1970 (unpublished).

³T. Fujii *et al.*, paper submitted to the Fifteenth International Conference on High-Energy Physics, Kiev, U.S.S.R., 1970 (unpublished).

⁴B. D'Almague, thesis, l'Université de Paris, Centre d'Orsay, 1970 (unpublished).

⁵R. L. Anderson *et al.*, Phys. Rev. Letters **23**, 725 (1969); see also **21**, 479 (1968).

⁶G. Buschorn *et al.*, Phys. Rev. Letters **20**, 230 (1968).

⁷M. Jacob and G. C. Wick, Ann. Phys. (N.Y.) **7**, 404 (1959).

⁸J. V. Beaupre and E. A. Paschos, Phys. Rev. D **1**, 2040 (1970).

⁹A detailed discussion of the apparatus and experimental method is contained in K. Ekstrand, Ph.D. thesis,

Cornell University, 1971 (unpublished).

¹⁰H. W. Koch and J. W. Motz, Rev. Mod. Phys. **31**, 920 (1959).

¹¹G. Lutz and H. D. Schulz, DESY Report No. 67/29, 1967 (unpublished).

¹²Science Accessories Corporation, 65 Station Street, Southport, Conn.

¹³R. Alvarez *et al.*, Phys. Rev. D **1**, 1946 (1970).

¹⁴N. I. Petrov *et al.*, Zh. Eksp. Teor. Fiz. **37**, 957 (1959) [Sov. Phys. JETP **10**, 682 (1960)]; V. G. Ikonov *et al.*, *ibid.* **37**, 863 (1959) [*ibid.* **10**, 615 (1960)]; V. T. Osipenkov and S. S. Filipov, *ibid.* **34**, 224 (1958) [*ibid.* **7**, 154 (1958)].

¹⁵R. Loe (private communication).

¹⁶V. Barger and P. Weiler, Phys. Letters **30B**, 105 (1969).

¹⁷R. D. Bajpaj, Lett. Nuovo Cimento **4**, 950 (1970).

¹⁸R. L. Kelly, G. L. Kane, and F. Henyey, Phys. Rev. Letters **24**, 1511 (1970).

¹⁹R. Dolén, D. Horn, and C. Schmid, Phys. Rev. **166**, 1768 (1968).

²⁰R. Anthony *et al.*, Phys. Rev. Letters **21**, 1605 (1968).

Interference Effects of $K^*(890)$ and $K^*(1420)$ Resonances with the Background*

M. Aguilar-Benitez, S. U. Chung, and R. L. Eisner
Brookhaven National Laboratory, Upton, New York 11973

(Received 22 February 1972)

We have made a study of interference effects between $K^*(890)$ and $K^*(1420)$ resonances and the background as observed in the reaction $K^-p \rightarrow K^- \pi^+ n$ at 3.9- and 4.6-GeV/c incident momenta, using a mass-dependent formalism which utilizes the generalized multipole moments. From this analysis we have obtained the $K^*(890)$ and $K^*(1420)$ density-matrix elements in the Jackson frame which satisfy the spin-1 and spin-2 positivity conditions, respectively. We discuss the implications of the degree and the phase of the interference on the nature of the production mechanism as well as the question of whether there exists a daughter resonance near the $K^*(1420)$.

I. INTRODUCTION

The purpose of this paper is to study interference effects between $K^*(890)$ and $K^*(1420)$ resonances and the background. Particular emphasis has been given to the problem of extracting den-

sity-matrix elements $\rho_{mm'}$ when the resonance interferes with the background.

This study has been motivated by the long-standing problem¹⁻³ that one of the diagonal density-matrix elements (i.e., ρ_{22}) for spin-2 resonances such as $f^0(1250)$ or $K^*(1420)$ is found to be nega-

tive with the conventional method of determining the $\rho_{mm'}$; the probabilistic nature of the density matrix demands, of course, that ρ_{mm} be positive for all m . In order to surmount this problem, we have allowed for the resonance to interfere with background using a formalism which takes into account the mass dependence of each partial wave present in a given mass region.

With this formalism, it should be possible in principle to measure all elements of the spin-2 density matrix; however, we find that, with our data, it is not possible to determine uniquely the $\rho_{mm'}$ for the $K^*(1420)$ resonance. Instead, we are led to determine the experimentally allowed ranges for each $\rho_{mm'}$ reflecting the ambiguity in the precise amount of interference between the resonance and background. Analysis of the forwardly produced $K^*(1420)$ events shows, however, that the amount of interference required to describe the data reaches the maximum allowable value and in this case the density-matrix elements can be determined uniquely. In particular, all $\rho_{mm'}$ for which m or m' is equal to 2 are found to be zero, indicating that spin-2 exchange is not an important component of the $K^*(1420)$ production mechanism.

We find from analysis of both the $K^*(890)$ and $K^*(1420)$ events that a large fraction of the forward resonance events tends to be coherent with the S-wave background. A likely explanation of this phenomenon is that both the resonances and the S wave arise from the same production mechanism. Vector-meson exchange cannot be responsible for the S-wave production, which leaves the π -exchange process as the only likely candidate for production of both the S wave and the resonances.

II. EXPERIMENTAL DATA

The data for this study come from an exposure of K^- beams at 3.9 and 4.6 GeV/c in the BNL 80-in. hydrogen bubble chamber. A systematic study of the production and decay of $K^*(890)$ and $K^*(1420)$ has been published elsewhere¹; for our purposes, we concentrate only on the following reactions:

$$K^-p \rightarrow K^{*0}(890)n \rightarrow K^- \pi^+ n, \quad (1a)$$

$$K^-p \rightarrow K^{*0}(1420)n \rightarrow K^- \pi^+ n. \quad (1b)$$

For this analysis, we have combined the 3.9- and 4.6-GeV/c data, since we find no essential difference between the two momenta. The sample so obtained consists of 9430 events in the reaction $K^-p \rightarrow K^- \pi^+ n$.

We show in Fig. 1 the effective-mass spectrum of the $K^- \pi^+$ [to be denoted $w(K^- \pi^+)$] for the combined data. A fit to this distribution using two Breit-Wigner shapes on a polynomial background

gives approximately 2800 $K^{*0}(890)$ events and 1500 $K^{*0}(1420)$ events. In Figs. 2(a) and 2(b) are displayed the t distribution for $K^{*0}(890)$ events and the t' distribution ($t' \equiv t - t_{\max}$) for $K^{*0}(1420)$ events, respectively, obtained from fits to the $w(K^- \pi^+)$ distribution for each t (or t') interval. It is seen that both K^* 's are produced via a peripheral mechanism (the slopes for each energy are given in Ref. 1).

In order to assess the partial-wave content in the $K^{*0}(890)$ region, we have examined the unnormalized Y_L^M moments as a function of $w(K^- \pi^+)$ in the interval between 0.7 and 1.1 GeV. (See Sec. III for a precise definition of the moments used in the present analysis.) All the moments up to $L=2$ are given in Figs. 3-8 (see Sec. IV) for six different t intervals; those with $L>2$ are found to be consistent with zero throughout the mass region. Although there are some indications that the extreme high-mass region contains some P wave not associated with the $K^{*0}(890)$, it can be seen that the resonating P wave plus a smooth S-wave background can give an excellent description of the data.

Turning to the partial-wave content in the $K^*(1420)$ region, we find that no statistically significant moment with $L>4$ exists in the $w(K^- \pi^+)$ interval between 1.1 and 1.7 GeV. Unnormalized even moments ($L=0, 2, \text{ and } 4$) which show significant deviation from zero anywhere in this mass interval are shown in Figs. 10-12 (see Sec. V) for three different t' intervals. It can be seen that no significant $L=4$ moments are found outside the

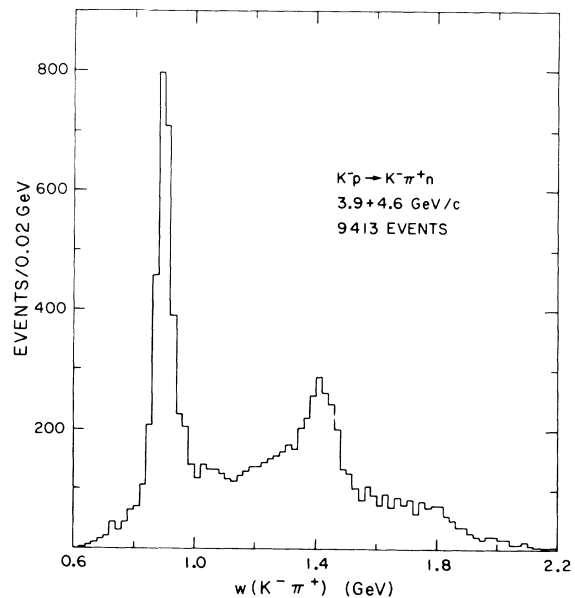


FIG. 1. $K^- \pi^+$ effective-mass distribution for reaction $K^-p \rightarrow K^- \pi^+ n$.

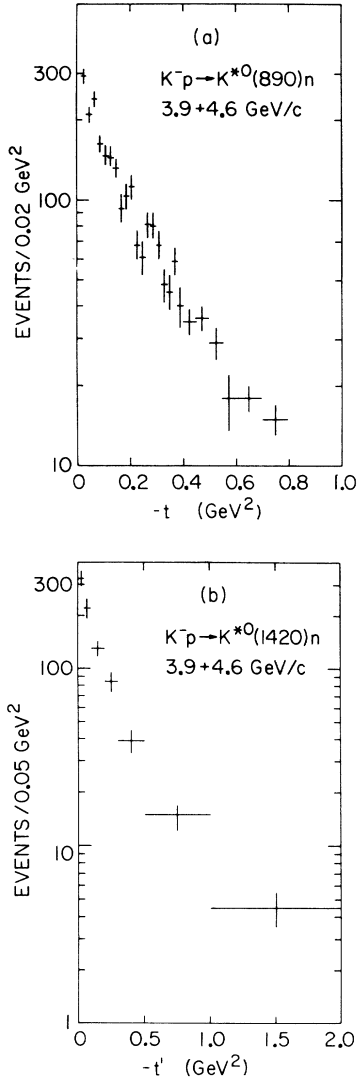


FIG. 2. (a) [(b)] $-t$ [$-t'$] distribution for $K^*(890)$ [$K^*(1420)$] events.

$K^*(1420)$ region (1.3–1.5 GeV), while small but statistically significant $L=2$ moments persist outside the $K^*(1420)$ region. From this observation, we conclude that an adequate description of the data can be achieved with a resonant D wave over a background composed of S and P waves.

III. THEORETICAL FORMULAS

In this section we present relevant theoretical formulas necessary for the partial-wave analysis of the $K^-\pi^+$ spectrum in the $K^*(1420)$ region. The analysis of the $K^*(890)$ region involves similar but simpler formulas.

We proceed with the hypothesis that three partial waves of spins s_1 , s_2 , and s_3 are necessary to describe a region of the $K^-\pi^+$ spectrum. Now, for a

given t interval, the $K^-\pi^+$ system is completely specified by three variables, the effective mass and the two angles (θ, φ) specifying the orientation of the $K^-\pi^+$ system, so that the differential cross sections may be written

$$\frac{d\sigma}{dw d\Omega} = \sum_{i=1}^3 \epsilon_i^2 |f_i(w)|^2 I_{ii}(\Omega) + 2 \sum_{i<j} \epsilon_i \epsilon_j \text{Re}\{f_i(w) f_j^*(w) I_{ij}(\Omega)\}, \quad (2)$$

where w is the $K^-\pi^+$ effective mass and $\Omega = (\theta, \varphi)$ stands for the Jackson angles of the $K^-\pi^+$ system.⁴ ϵ_i^2 is the fraction of the s_i wave in a given w interval (defined by the limits w_a and w_b), and $|f_i(w)|^2$ represents the mass dependence of the s_i wave, normalized according to

$$\int_{w_a}^{w_b} dw |f_i(w)|^2 = 1. \quad (3)$$

In Eq. (2) we have assumed that the amplitude representing a given partial wave can be *factorized* into two terms, one containing the mass dependence [i.e., $f_i(w)$] and the other containing the information on the angular dependence. Thus, $I_{ii}(\Omega)$ represents the angular dependence of the s_i wave, while $I_{ij}(\Omega)$ specifies the interference between the s_i and s_j waves. They may be written succinctly by⁵

$$I_{ij}(\Omega) = \sum_{LM} \left(\frac{2L+1}{4\pi} \right) H_{ij}(LM) D_{M0}^L(\Omega), \quad i, j = 1, 2, 3 \quad (4)$$

where $|s_i - s_j| \leq L \leq s_i + s_j$ and $-L \leq M \leq +L$. D_{mm}^L is the usual D function as defined in Rose⁶ and $H_{ij}(LM)$ is the “partial” moment (resulting from the interference between spins s_i and s_j) defined by

$$H_{ij}(LM) = \int d\Omega I_{ij}(\Omega) D_{M0}^L(\Omega) = \left(\frac{4\pi}{2L+1} \right)^{1/2} \int d\Omega I_{ij}(\Omega) Y_L^M(\Omega) [Y_L^M(\Omega) \text{ is the spherical harmonic}]. \quad (5)$$

We shall denote by $H(LM)$ the over-all moment that can actually be determined experimentally:

$$\frac{dH(LM)}{dw} = \int d\Omega \frac{d\sigma}{dw d\Omega} D_{M0}^L(\Omega) = \sum_{i=1}^3 \epsilon_i^2 |f_i(w)|^2 H_{ii}(LM) + 2 \sum_{i<j} \epsilon_i \epsilon_j \text{Re}\{f_i(w) f_j^*(w) H_{ij}(LM)\}. \quad (6)$$

Note that $H_{ij}(LM)$ is by definition independent of mass w , and the mass dependence of $dH(LM)/dw$ is contained in $f_i(w)$. The unnormalized experimental moment, to be denoted $NH(LM)$, is related to the differential moment defined above via

$$NH(LM)|_{\Delta w} = N \int_{\Delta w} \frac{dH(LM)}{dw} dw = \sum_i D_{i0}^L(\Omega_i), \quad (7)$$

where the sum extends over all events in a given mass bin of width Δw and N is the total number of events in the mass interval between w_a and w_b . Note that with this definition of experimental moments the $NH(00)$ moment simply represents the mass spectrum.

The moments $H_{ij}(LM)$ are normalized according to

$$H_{ij}(00) = \delta_{ij} \quad (8a)$$

so that the angular distribution has the normalization

$$\int d\Omega I_{ij}(\Omega) = \delta_{ij}. \quad (8b)$$

Combining (2) and (8), we see that the over-all normalization of the differential cross section is fixed by

$$\int_{w_a}^{w_b} dw \int d\Omega \frac{d\sigma}{dw d\Omega} = \epsilon_1^2 + \epsilon_2^2 + \epsilon_3^2 = 1. \quad (9)$$

The moments $H_{ij}(LM)$ have the following expansion in terms of the density matrix:

$$H_{ij}(LM) = \left(\frac{2s_i + 1}{2s_i + 1} \right)^{1/2} \sum_{mm'} \rho_{mm'}^{(ij)} (s_j m' LM | s_i m) \times (s_j 0 L 0 | s_i 0), \quad (10)$$

where we have used the notation $(l_1 m_1 l_2 m_2 | l_3 m_3)$ for the Clebsch-Gordan coefficients and $\rho_{mm'}^{(ij)}$ are the *generalized* density-matrix elements (see Appendix A); $\rho_{mm'}^{(ii)}$ is the usual density-matrix element for a spin- s_i system, and $\rho_{mm'}^{(ij)}$ for $i \neq j$ represents the interference between the states $|s_i m\rangle$ and $|s_j m'\rangle$. Hermiticity of the density matrix demands that

$$\rho_{mm'}^{(ij)} = \rho_{m'm}^{(ji)*}, \quad (11)$$

while parity conservation in the production process leads to the relations (valid if the quantization axis is in the production plane)

$$\rho_{mm'}^{(ij)} = (-)^{m-m'} \rho_{-m-m'}^{(ij)}. \quad (12)$$

Formulas (11) and (12) in turn lead to the following

relations among the moments:

$$H_{ij}(LM) = (-)^M H_{ji}^*(L-M), \quad (13)$$

$$H_{ij}(LM) = (-)^{s_i - s_j} (-)^{L+M} H_{ij}(L-M). \quad (14)$$

These relations plus Eq. (10) show that the moments $H_{ii}(LM)$ are real if $L = \text{even}$ and zero if $L = \text{odd}$, while the interference moments $H_{ij}(LM)$ ($i \neq j$) are complex (zero) if $s_i - s_j + L = \text{even}$ (odd).

It should be noted that the moments $H_{ij}(LM)$ are not all independent; there are certain inequalities that have to be satisfied among the $H_{ii}(LM)$'s due to the positivity conditions of the density matrix (see Appendix A). In addition, there exist inequalities for $H_{ij}(LM)$ for $i \neq j$ that arise from the following relationship among the density-matrix elements:

$$|\rho_{mm'}^{(ij)}|^2 \leq \rho_{mm}^{(ii)} \rho_{m'm}^{(jj)}. \quad (15)$$

The interference moments between the spins $s_i = J$ and $s_j = 0$ are of particular importance for our purposes. They can be parametrized by taking advantage of the inequality (15), i.e.,

$$H_{J0}(Jm) = r_m e^{i\alpha_m} [\rho_{mm}^{(J)} / (2J+1)]^{1/2}, \quad (16)$$

where $0 \leq r_m \leq 1$ and $0 \leq \alpha_m \leq 2\pi$ and $\rho_{mm}^{(J)}$ is the diagonal density-matrix element for the spin- J system (see Appendix B). Thus, $r_m = 1$ ($r_m = 0$) corresponds to the maximum (zero) interference between the states $|Jm\rangle$ and $|00\rangle$.

We now present a symmetry relation which greatly simplifies the analysis of the interference effects. Relation (14) implies that the angular distribution given by Eq. (4) has the following symmetry:

$$I_{ij}(\pi - \theta, \pi - \varphi) = (-)^{s_i - s_j} I_{ij}(\theta, \varphi). \quad (17)$$

If we "symmetrize" the experimental data by the operation $(\theta, \varphi) \rightarrow (\pi - \theta, \pi - \varphi)$, then the corresponding theoretical distribution defined by

$$\left. \frac{d\sigma}{dw d\Omega} \right|_{\text{sym}} = \frac{1}{2} \left(\frac{d\sigma}{dw d\Omega}(\theta, \varphi) + \frac{d\sigma}{dw d\Omega}(\pi - \theta, \pi - \varphi) \right) \quad (18)$$

does not contain those interference terms $I_{ij}(\Omega)$ for which $s_i - s_j$ is odd. This means, for instance, that, if we symmetrize the experimental data in the $K^{*0}(890)$ region, the corresponding angular distribution involves the squares of S- and P-wave amplitudes but no S-P interference term. Therefore, a system consisting of S and P waves can be analyzed without ever explicitly knowing the interference terms. On the other hand, it is impossible to analyze a system composed of S and D waves without introducing the interference terms.

In Sec. IV, we shall analyze the $K^{*0}(890)$ region

without symmetrizing the data, since we have sufficient statistics to accommodate the four additional parameters which come from inclusion of the S - P interference term. On the other hand, the analysis of the $K^*(1420)$ region involves such a large number of parameters that it was found necessary to symmetrize the experimental data according to Eq. (18); the theoretical distribution function so obtained included the squares of the S -, P -, and D -wave amplitudes as well as the S - D interference term. Had we included the S - P and P - D interference terms, we would have had to contend with 16 additional parameters.

A slightly different aspect of this problem is worth emphasizing. Insofar as the determination of the $K^*(1420)$ density matrix is concerned, the S - D interference term ought to be considered "intrinsic," for there is no way to separate it from the D -wave angular distribution. The S - P and P - D interference terms, on the other hand, have "odd" symmetry [in the sense of Eq. (17)], and it is not necessary to know them to extract the $K^*(1420)$ density matrix.

IV. ANALYSIS OF THE $K^*(890)$ REGION

We have seen that the region of $w(K^-\pi^+)$ from 0.7 to 1.1 GeV can be represented by S and P waves. For this case the distribution function can be written

$$\frac{d\sigma}{dw d\Omega} = \epsilon_S^2 |f_S(w)|^2 I_S(\Omega) + \epsilon_P^2 |f_P(w)|^2 I_P(\Omega) + 2\epsilon_P \epsilon_S \operatorname{Re}\{f_P(w) f_S^*(w) I_{PS}(\Omega)\}, \quad (19)$$

where

$$I_S(\Omega) = \frac{1}{4\pi}, \quad (20a)$$

$$I_P(\Omega) = \frac{1}{4\pi} \left(1 + \sum_{M=0}^2 H_P(2M) B_M^2(\Omega) \right), \quad (20b)$$

$$I_{PS}(\Omega) = \frac{1}{4\pi} \sum_{M=0}^1 H_{PS}(1M) B_M^1(\Omega), \quad (20c)$$

and

$$B_M^L(\Omega) = (2 - \delta_{M0})(2L+1) d_{M0}^L(\theta) \cos M\varphi. \quad (20d)$$

See Berman and Jacob⁷ for explicit formulas for $d_{MM'}^L$. Note that we have simplified the notations of Sec. III by writing $I_P(\Omega)$ or $H_P(LM)$ for $I_{ii}(\Omega)$ or $H_{ii}(LM)$. Formula (19), when integrated over w in the resonance region, reduces to the familiar form of the S - P wave angular distributions applicable to $J^P = 1^-$ resonance decay.⁸

Equation (20b) shows that the square of the P -wave amplitude involves three real parameters $H_P(20)$, $H_P(21)$, and $H_P(22)$, which may be related

to the familiar density-matrix elements via Eq. (10). (For explicit relations, see Appendix B.) The S - P interference term $I_{PS}(\Omega)$ depends on two complex parameters $H_{PS}(10)$ and $H_{PS}(11)$. Together with the parameter ϵ_S^2 [the fraction of S wave in the $w(K^-\pi^+)$ interval 0.7 to 1.1 GeV] and the slope of $f_S^2(w)$, we see that the analysis of the $K^*(890)$ region requires nine real parameters.

In the analysis, the function $f_S(w)$ was assumed real, and $f_S^2(w)$ was assumed to be a straight line whose slope was essentially determined by the relative height of the mass distributions near 0.7 and 1.1 GeV. For the function $f_P(w)$, we have used the standard S -wave Breit-Wigner formula with the $K^*(890)$ mass and width¹ set at $w_0 = 896$ MeV and $\Gamma = 55$ MeV, respectively, i.e.,

$$f_P(w) = \delta_0 e^{i\delta(w)} \sin \delta(w), \quad (21)$$

$$\cot \delta(w) = (w_0^2 - w^2)/(w_0 \Gamma),$$

where δ_0 is the normalization constant [see Eq. (3)]. It is not necessary for our purposes to use a more elaborate form for $f_P(w)$ such as the P -wave Breit-Wigner formula, because it only amounts to taking a slightly shifted mass and width for the $K^*(890)$ and, possibly, a slightly different slope for the S -wave background. We are now ready to write the interference term in Eq. (19) more explicitly:

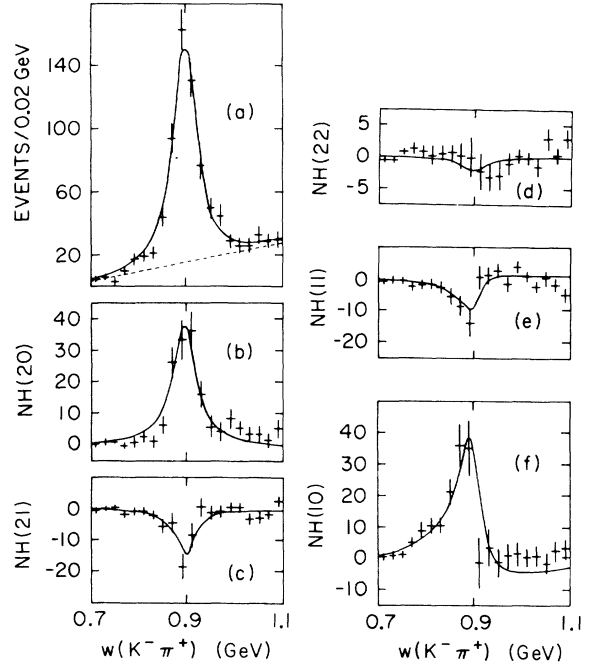


FIG. 3. (a)–(f) $NH(LM)$ moments in the $K^*(890)$ region for $-t < 0.05$ GeV². The solid curves are the results of the best fit. The dotted line in (a) represents the level of the S -wave background.

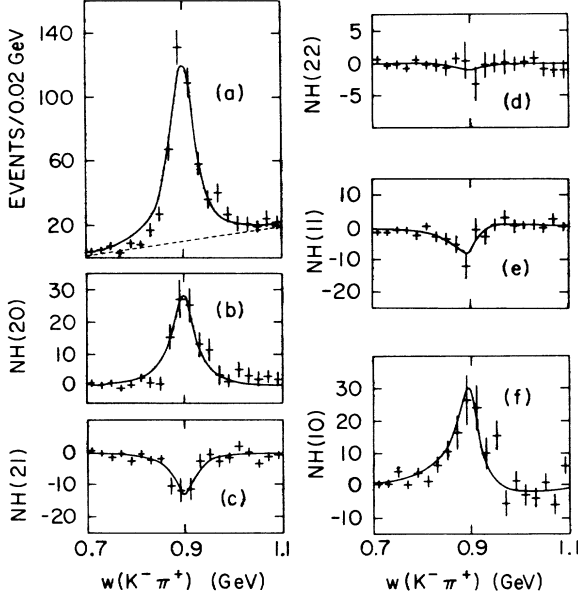


FIG. 4. (a)–(f) Same as Fig. 3 but for $0.05 < -t < 0.1$ GeV^2 .

$$\frac{d\sigma}{dw d\Omega} \Big|_{\text{int}} = \frac{\epsilon_P \epsilon_S}{2\sqrt{3} \pi} f_S(w) \delta_0 \sin \delta(w) \times \{ [\rho_{00}^{(P)}]^{1/2} r_0 \cos[\alpha_0 + \delta(w)] B_0^1(\Omega) + [\rho_{11}^{(P)}]^{1/2} r_1 \cos[\alpha_1 + \delta(w)] B_1^1(\Omega) \}, \quad (22)$$

where we have parametrized the interference mo-

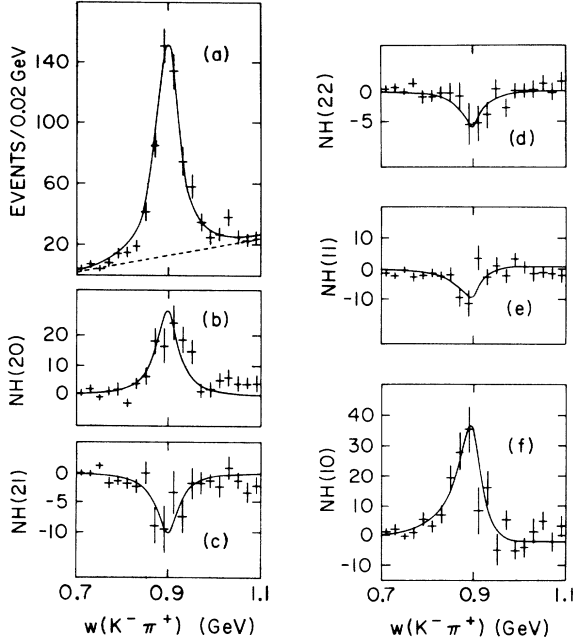


FIG. 5. (a)–(f) Same as Fig. 3 but for $0.1 < -t < 0.2$ GeV^2 .

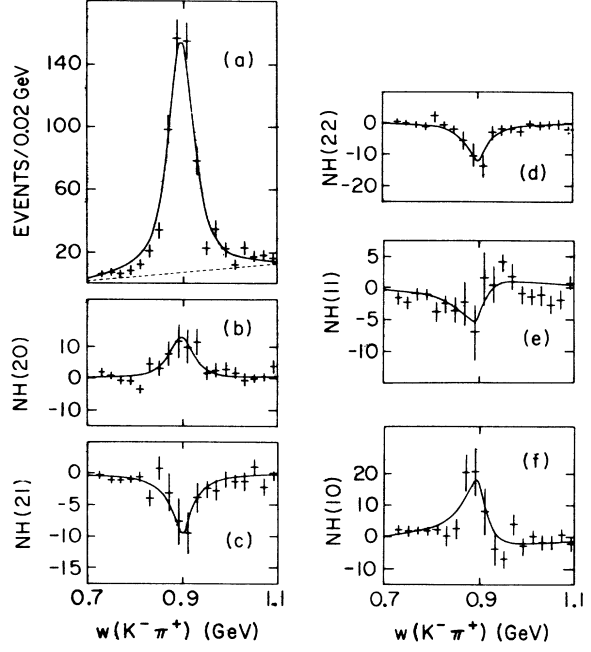


FIG. 6. (a)–(f) Same as Fig. 3 but for $0.2 < -t < 0.4$ GeV^2 .

ments $H_{PS}(1M)$ as in Eq. (16).

For each given t interval, we have fitted the data with the distribution function (19) by the maximum-likelihood method.⁹ The fitting procedure involved four stages: First, we fitted the mass spectrum by varying the amount of S -wave background as well as the slope; second, for fixed mass spectrum, we varied the resonance parameters $H_P(20)$, $H_P(21)$, and $H_P(22)$ with the interfer-

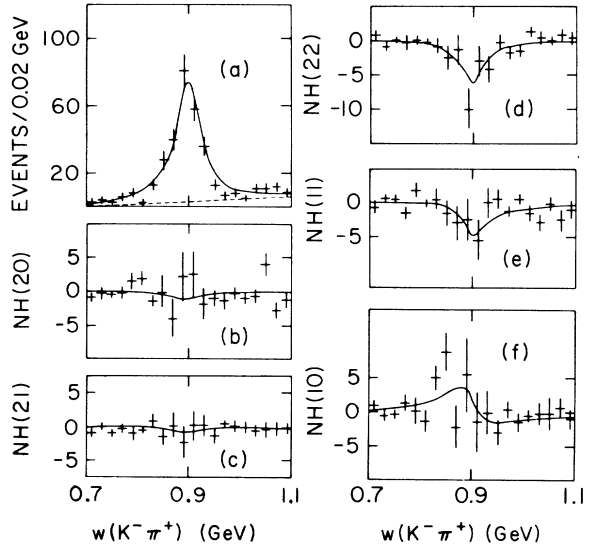


FIG. 7. (a)–(f) Same as Fig. 3 but for $0.4 < -t < 0.6$ GeV^2 .

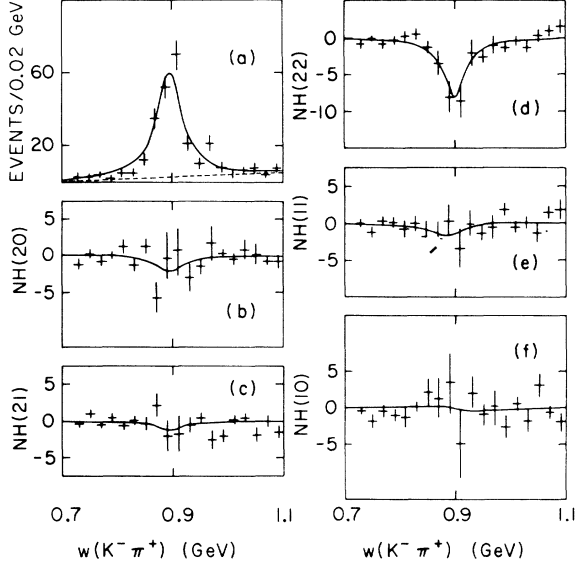


FIG. 8. (a)–(f) Same as Fig. 3 but for $0.6 < -t < 1.0$ GeV^2 .

ence parameters set to zero; third, the interference term was added to the fit; fourth and finally, all nine parameters were varied simultaneously. We have found that the fourth step is not in fact necessary; the parameters remained within 1 standard deviation of those found at the third stage.

The results of the fit are compared with the unnormalized moments $NH(LM)$ defined by Eq. (7). For each of six t intervals, we have plotted $NH(LM)$ for L up to 2 in Figs. 3–8, and the fitted distributions are shown as solid curves in each of these figures. It can be seen that the fits are good in all the t regions. A small but systematic deviation in some $NH(LM)$ in the high-mass region indicates that there may exist a small nonresonant P -wave background in this mass region. The dotted line shown in each of the mass spectra represents the amount of the S wave found in the fit.

In all the fits, the positivity conditions on the $K^*(890)$ density matrix [see (A14)] have been imposed. In addition, the upper limits on the interference density-matrix elements have been taken into account by requiring $r_m \leq 1$ [see Ref. 20 for comments on possible additional constraints]. Fitted values for r_m and α_m as well as the density-matrix elements evaluated in the Jackson frame are shown in Fig. 9 and Table I as a function of t .

We observe a large value of ρ_{00} (~ 0.8) at small $-t$, which indicates that the pion exchange is an important component in the $K^*(890)$ production process in our data.¹⁰ As can be seen, r_0 is also large at small $-t$ ($r_0 \gtrsim 95\%$), which means that the P wave in the state $|10\rangle$ tends to be coherent with

the S -wave background. In other words, the mechanism involved in the $K^*(890)$ production is also responsible for the S -wave production.

The values of the density-matrix elements ρ_{00} , ρ_{1-1} , and $\text{Re}\rho_{10}$ found in this analysis are consistent with those obtained earlier.¹⁰ The improvements in the present analysis are: (a) mass-dependent distribution has been used; (b) the S -wave fraction is a parameter in the fit, so that one is able to determine directly the elements ρ_{00} and ρ_{11} instead of the combination $\rho_{00}-\rho_{11}$; (c) one determines qualitatively the “degree of coherence” r_0 and r_1 ; and (d) one obtains the phase of the interference α_0 and α_1 .

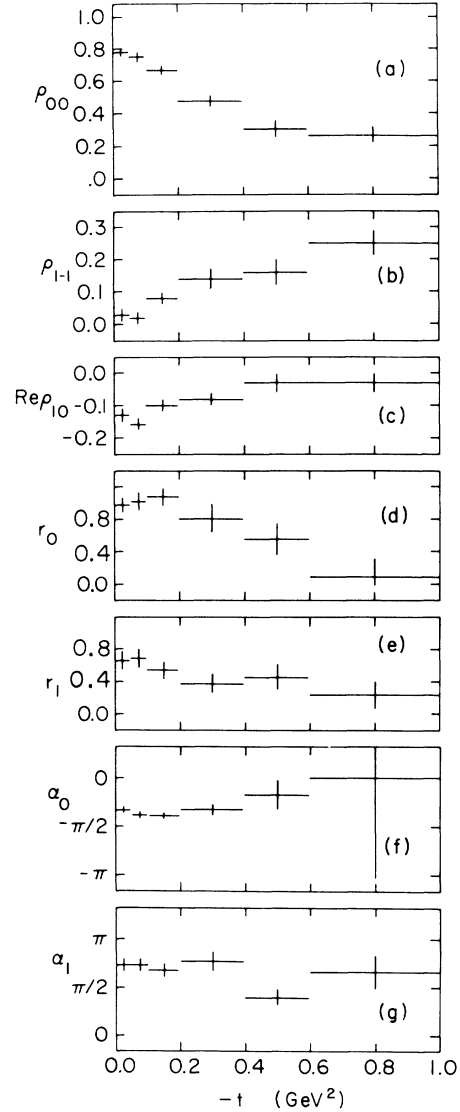


FIG. 9. (a)–(g) $K^*(890)$ density-matrix elements and interference parameters (r_0 , α_0 , r_1 , α_1) in the Jackson frame as a function of momentum transfer squared ($-t$).

TABLE I. $K^{*0}(890)$ density-matrix elements (Jackson frame) in reaction $K^-p \rightarrow K^{*0}(890)n$.

$ t $ (GeV ²)	Events ^a	$K^{*0}(890)$ events ^a	ρ_{00}	ρ_{1-1}	$\text{Re}\rho_{10}$	r_0	α_0	r_1	α_1
0.0 -0.05	858	581 ± 22	0.78 ± 0.03	0.03 ± 0.02	-0.13 ± 0.02	0.95 ± 0.10	-1.00 ± 0.08	0.64 ± 0.12	2.18 ± 0.18
0.05-0.1	655	458 ± 19	0.75 ± 0.03	0.02 ± 0.02	-0.16 ± 0.02	0.98 ± 0.12	-1.15 ± 0.08	0.66 ± 0.12	2.19 ± 0.16
0.1 -0.2	812	578 ± 21	0.67 ± 0.03	0.08 ± 0.02	-0.10 ± 0.02	0.98 ± 0.12	-1.16 ± 0.07	0.52 ± 0.12	2.04 ± 0.18
0.2 -0.4	748	620 ± 18	0.48 ± 0.03	0.14 ± 0.03	-0.08 ± 0.02	0.79 ± 0.18	-0.98 ± 0.15	0.37 ± 0.12	2.35 ± 0.31
0.4 -0.6	359	288 ± 14	0.31 ± 0.05	0.16 ± 0.04	-0.03 ± 0.03	0.54 ± 0.20	-0.51 ± 0.44	0.44 ± 0.16	1.18 ± 0.26
0.6 -1.0	282	231 ± 11	0.27 ± 0.05	0.25 ± 0.04	-0.03 ± 0.03	0.10 ± 0.22	0.04 ± 3.10	0.23 ± 0.18	1.97 ± 0.54

^a Events in the region $0.7 \leq w(K^- \pi^+) \leq 1.1$ GeV.

V. ANALYSIS OF THE $K^{*0}(1420)$ REGION

As pointed out in Sec. II, the $w(K^- \pi^+)$ region between 1.1 and 1.7 GeV can be described by a resonating D wave plus a background composed of S and P waves. It can be shown by using formulas (2) and (4) that, in addition to the parameters related to the mass spectrum, a complete analysis of the $K^- \pi^+$ system involves a total of 33 parameters. In order to reduce this number to a more manageable level, we have symmetrized both the experimental data¹¹ and the distribution function by the prescription (18):

$$\left. \frac{d\sigma}{dw d\Omega} \right|_{\text{sym}} = \epsilon_S^2 |f_S(w)|^2 I_S(\Omega) + \epsilon_P^2 |f_P(w)|^2 I_P(\Omega) + \epsilon_D^2 |f_D(w)|^2 I_D(\Omega) + 2\epsilon_D \epsilon_S \text{Re}\{f_D(w) f_S^*(w) I_{DS}(\Omega)\}, \quad (23)$$

where I_S and I_P are given by (20a) and (20b), and

$$I_D(\Omega) = \frac{1}{4\pi} \left(1 + \sum_{M=0}^2 H_D(2M) B_M^2(\Omega) + \sum_{M=0}^4 H_D(4M) B_M^4(\Omega) \right), \quad (24a)$$

$$I_{DS}(\Omega) = \frac{1}{4\pi} \sum_{M=0}^2 H_{DS}(2M) B_M^2(\Omega). \quad (24b)$$

$B_M^L(\Omega)$ is the same as that given in Eq. (20d).

Equation (24a) shows that the D -wave angular distribution depends on eight real parameters $H_D(2M)$ and $H_D(4M)$. These are related to the eight density-matrix elements $\rho_{mm}^{(D)}$, as shown in Appendix B. On the other hand, Eq. (24b), which describes the S - D interference effect, depends on three complex parameters $H_{DS}(2M)$. Together with the three real parameters required to describe $I_P(\Omega)$, a total of 17 real parameters are needed to describe the angular distributions of Eq. (23).

We now explicitly write the experimental moments in terms of the partial moments $H_{ij}(LM)$. From Eq. (6), we obtain

$$\frac{dH(4M)}{dw} = \epsilon_D^2 |f_D(w)|^2 H_D(4M), \quad (25a)$$

$$\begin{aligned} \frac{dH(2M)}{dw} &= \epsilon_P^2 |f_P(w)|^2 H_P(2M) + \epsilon_D^2 |f_D(w)|^2 H_D(2M) \\ &\quad + 2\epsilon_D \epsilon_S \text{Re}\{f_D(w) f_S^*(w) H_{DS}(2M)\} \\ &= \epsilon_P^2 f_P^2(w) H_P(2M) + \epsilon_D^2 \delta_0^2 \sin^2 \delta(w) H_D(2M) \\ &\quad + \frac{2}{\sqrt{5}} \epsilon_D \epsilon_S f_S(w) \delta_0 \sin \delta(w) [\rho_{MM}^{(D)}]^{1/2} \\ &\quad \times r_M \cos[\alpha_M + \delta(w)], \end{aligned} \quad (25b)$$

where we have assumed that $f_S(w)$ and $f_P(w)$ are real and $f_D(w)$ has the same Breit-Wigner form as that given in Eq. 21. The interference moments $H_{DS}(2M)$ have been reexpressed using formula (16).

It can be seen from Eq. (25a) that $H_D(4M)$ can be uniquely determined, once ϵ_D and $f_D(w)$ are known. However, the experimental moment $H(2M)$ has contributions from three different sources: $H_D(2M)$ from the resonant D wave, $H_P(2M)$ from the P -wave background, and $H_{DS}(2M)$ from the S - D interference.

Assuming that the P -wave background has smooth mass dependence throughout the $K^*(1420)$ region, we can uniquely determine $H_P(2M)$ by observing the behavior of $dH(2M)/dw$ outside the $K^*(1420)$ region.

However, it is not always possible to distinguish $H_D(2M)$ from $H_{DS}(2M)$. As can be seen in formula (25b), if α_M is near $\pm \frac{1}{2}\pi$, the mass dependence of the S - D interference term can behave like the resonance term $|f_D(w)|^2$ [this is true as long as $f_S(w)$ does not have violent mass-dependence near the resonance]. In this particular case, one can only determine the ranges for $H_D(2M)$'s (and consequently the ranges for $\rho_{mm}^{(D)}$). This is precisely what happens with our present experimental data. The most prominent moment in our data, the $NH(20)$ moment, has a mass dependence of the Breit-Wigner shape with mass and width very nearly those found in the mass spectrum. Because of this, we find experimentally that α_0 is near $\pm \frac{1}{2}\pi$, and we are led to determine only the ranges for $H_D(2M)$'s.

For the mass dependence of the resonance, we have used the S -wave Breit-Wigner shape with the $K^*(1420)$ parameters¹ fixed at $w_0 = 1420$ MeV and

$\Gamma=120$ MeV. [See Eq. (21).] We have chosen to parametrize the background mass dependence by three straight lines, and the resulting fits are shown in Figs. 10, 11, and 12. It should be pointed out that this procedure is nearly as good as a smooth polynomial fit to the background; it can be seen in Fig. 10(a), for instance, that the straight lines approximate well the curve with open circles, which has been obtained by fitting the background to a polynomial shape.

The normalized mass dependence of the background, to be denoted by $f_B^2(w)$, is related to those of the S and P waves via

$$(\epsilon_S^2 + \epsilon_P^2)f_B^2(w) = \epsilon_S^2 f_S^2(w) + \epsilon_P^2 f_P^2(w), \quad (26)$$

where f_B , f_S , and f_P are assumed real. Experimentally, we find that the only significant background moment is $NH(20)$. Making the simple assumption that the P-wave mass dependence, $f_P(w)$, can be approximated by a straight line, we have determined its slope by examining the $NH(20)$ moment outside the $K^*(1420)$ region. The S-wave mass dependence can then be fixed through Eq. (26), once $f_B(w)$ and $f_P(w)$ have been determined.

From this discussion, we see that there are a total of six parameters related to the mass spectrum, i.e., three slopes for $f_B^2(w)$, one slope for $f_P^2(w)$, ϵ_D^2 , and ϵ_P^2 . Together with the 17 parameters required to describe the angular distribution, the analysis of the $K^*(1420)$ region involves a total of 23 parameters. As was the case for the $K^*(890)$ analysis, we have used the maximum-

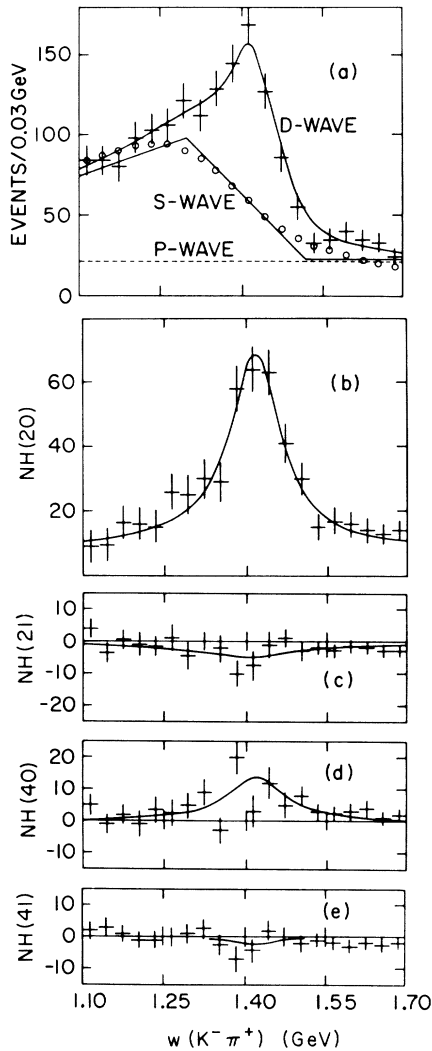


FIG. 10. (a)–(e) $NH(LM)$ moments in the $K^*(1420)$ region for $-t' < 0.1$ GeV². The solid curves are the results of the best fit. The solid lines (dotted line) represent the background level (P -wave level). The curve with open circles represents an alternative polynomial fit to the background.

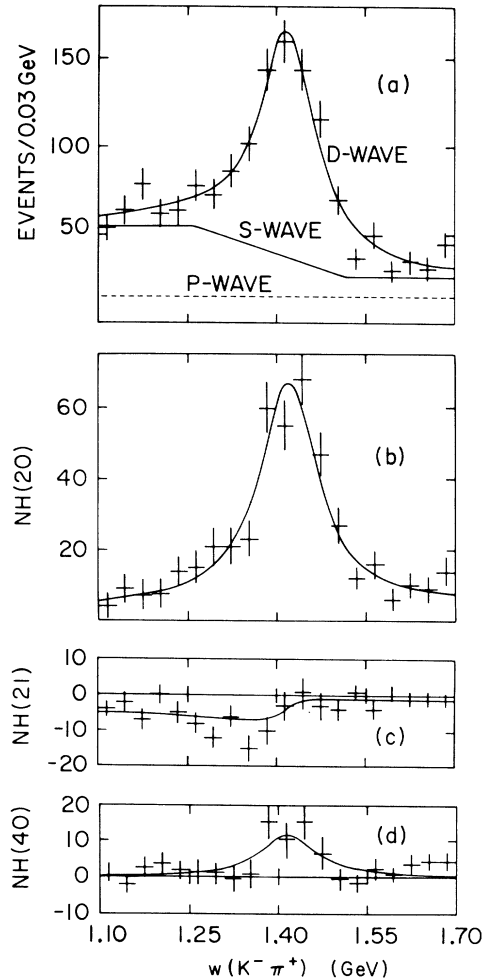


FIG. 11. (a)–(d) Same as Fig. 10 but for $0.1 < -t' < 0.5$ GeV².

likelihood method⁹ to determine these parameters. The fitting procedure involved seven distinct stages, as follows:

(1) Determine the $K^*(1420)$ fraction ϵ_D^2 and the shape of the background spectrum $f_B^2(w)$.

(2) With the S-D interference terms fixed at zero, determine the slope of $f_P^2(w)$, the P-wave fraction ϵ_P^2 , and the values of $H_P(2M)$, $H_D(2M)$, and $H_D(4M)$. This procedure leads to a value of $\rho_{22}^{(D)}$ which is significantly negative for all l' intervals [see Table III(a), below],¹² demonstrating the need for S-D interference effects. In subsequent stages, we fix the P-wave parameters as found at this stage and introduce the interference terms $H_{DS}(2M)$ in the fit to obtain the limiting values of $H_D(2M)$.

(3) In order to obtain the maximum value of $H_D(20)$, we set $\rho_{22}^{(D)} = 0$ and vary α_0 (starting value $= -\frac{1}{2}\pi$) and r_0 of $H_{DS}(20)$. Note that in this case $H_D(20)$ is related to $H_D(40)$ [see formula (B5)], i.e.,

$$H_D(20) = \frac{1}{5} \left[1 + \frac{3}{2} H_D(40) \right]. \quad (27)$$

(4) Set $r_0 = 1$ and vary $H_D(20)$ and α_0 (starting value $= -\frac{1}{2}\pi$) to maximize the likelihood; this procedure gives the minimum $H_D(20)$ and leads to a positive value for $\rho_{22}^{(D)}$.

(5) As can be seen in Figs. 10–12, the moments $H(21)$ and $H(22)$ are small throughout the $K^*(1420)$ region. There is the possibility that this situation arises from cancellation of a large positive (negative) $H_D(2M)$ moment with equally large negative (positive) $H_{DS}(2M)$ moment. Therefore, the limiting values of $H_D(21)$ or $H_D(22)$ have been obtained by setting $r_1 = r_2 = 1$ and by varying $H_D(21)$, $H_D(22)$, and the phases α_1 and α_2 . This procedure leads to a maximum or minimum value of $H_D(2M)$ depending on whether the starting value of α_M has been set at $+\frac{1}{2}\pi$ or $-\frac{1}{2}\pi$.

(6) Investigate the uniqueness of fit by varying different sets of parameters, e.g., minimum $H_D(21)$ with maximum $H_D(22)$, etc.

(7) If the limiting values of $H_D(2M)$ together with $H_D(4M)$ are used to obtain the corresponding limiting values of $\rho_{mm}^{(D)}$, it is found that the full spin-2 positivity conditions of Eqs. (A23) to (A28) are grossly violated, even though $\rho_{22}^{(D)}$ is non-negative. In order to avoid this problem, we have progressively reduced the ranges of $H_D(2M)$ until the positivity conditions can be satisfied. The quoted experimental ranges for $\rho_{mm}^{(D)}$ in Tables III(b) and III(c) below have been obtained in this manner.

In all the fits, we have imposed the spin-1 positivity conditions (A14) on the P-wave background moments $H_P(2M)$. It should be noted that the parameters ϵ_S^2 , ϵ_P^2 , and $H_P(2M)$ can be uniquely determined as long as the mass spectra $f_S^2(w)$ and $f_P^2(w)$ are significantly different. If this is not the case, one can only determine the combination $\epsilon_P^2 H_P(2M)$. This can be seen by writing down the angular distribution functions for the case $f_S^2(w) = f_P^2(w)$ from Eq. (23); the background angular distribution is then proportional to

$$\begin{aligned} & \epsilon_S^2 I_S(\Omega) + \epsilon_P^2 I_P(\Omega) \\ &= \frac{1}{4\pi} \left(1 - \epsilon_D^2 + \sum_M \epsilon_P^2 H_P(2M) B_M^2(\Omega) \right). \end{aligned} \quad (28)$$

We find experimentally that, for the first two l' intervals, $f_S^2(w)$ and $f_P^2(w)$ have sufficiently different shapes so that it is possible to determine uniquely ϵ_P^2 and $H_P(2M)$. On the other hand, for the third l' interval the likelihood function turns out to be relatively flat when plotted as a function of ϵ_P^2 . We have chosen the minimum value of ϵ_P^2 for which one obtains a good fit to the data. This value corresponds to the maximum amount of S

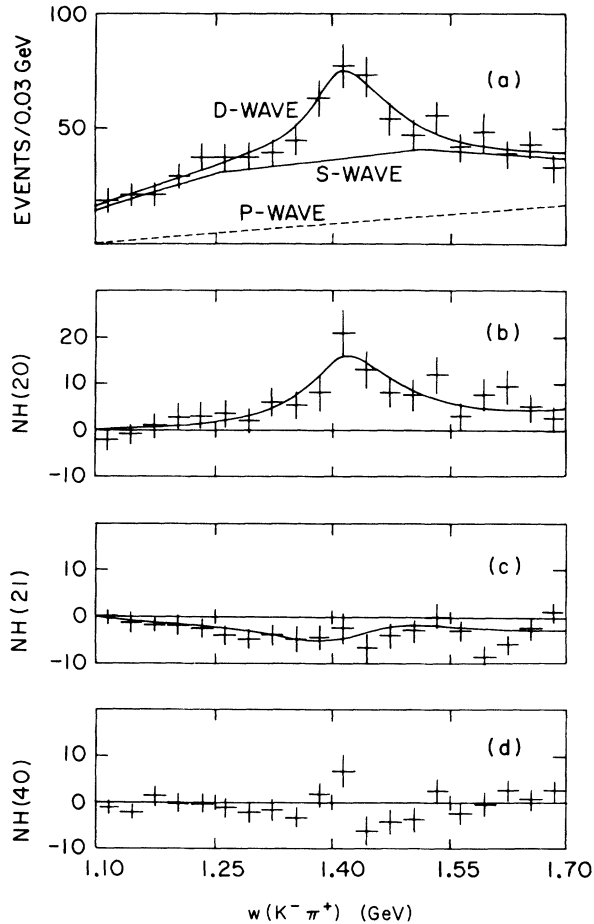


FIG. 12. (a)–(d) Same as Fig. 10 but for $0.5 < -t < 2.0$ GeV^2 .

TABLE II. Fitted moment for three regions of $|t'|$.

(a) $ t' \leq 0.1 \text{ GeV}^2$.			
Events ^a	1700		
$K^*(1420)$ events ^a	530 ± 51		
ϵ_D^2	0.31 ± 0.03	$H_D(40)$	0.14 ± 0.04
ϵ_P^2	0.27 ± 0.02	$H_D(41)$	-0.02 ± 0.03
$H_P(20)$	0.39 ± 0.02	$H_D(42)$	-0.01 ± 0.02
$H_P(21)$	-0.05 ± 0.02	$H_D(43)$	0.0 ± 0.02
$H_P(22)$	0.0 ± 0.02	$H_D(44)$	0.0 ± 0.04
	Minimum	Maximum	No interference
$H_D(20)$	0.24 ± 0.03	0.24 ± 0.01	0.58 ± 0.04
r_0	1.0	0.97 ± 0.12	0.0
α_0	4.43 ± 0.12	4.43 ± 0.12	0.0
$H_D(21)$	-0.19 ± 0.03	0.15 ± 0.03	-0.04 ± 0.02
r_1	1.0	1.0	0.0
α_1	4.46 ± 0.18	1.33 ± 0.18	0.0
$H_D(22)^b$	0.0 ± 0.02	0.0 ± 0.02	0.0 ± 0.02
r_2	0.0	0.0	0.0
α_2	0.0	0.0	0.0
(b) $0.1 \leq t' \leq 0.5 \text{ GeV}^2$.			
Events ^a	1518		
$K^*(1420)$ events ^a	703 ± 45		
ϵ_D^2	0.46 ± 0.03	$H_D(40)$	0.10 ± 0.02
ϵ_P^2	0.19 ± 0.02	$H_D(41)$	0.01 ± 0.02
$H_P(20)$	0.31 ± 0.03	$H_D(42)$	-0.02 ± 0.02
$H_P(21)$	-0.17 ± 0.02	$H_D(43)$	-0.01 ± 0.02
$H_P(22)$	0.04 ± 0.02	$H_D(44)$	0.0 ± 0.02
	Minimum	Maximum	No interference
$H_D(20)$	0.20 ± 0.02	0.23 ± 0.01	0.49 ± 0.04
r_0	1.0	0.88 ± 0.22	0.0
α_0	4.49 ± 0.12	4.53 ± 0.12	0.0
$H_D(21)$	-0.18 ± 0.02	0.16 ± 0.02	-0.02 ± 0.02
r_1	1.0	1.0	0.0
α_1	4.30 ± 0.14	1.77 ± 0.14	0.0
$H_D(22)$	-0.07 ± 0.02	0.06 ± 0.02	0.0 ± 0.02
r_2	1.0	1.0	0.0
α_2	4.51 ± 0.32	1.56 ± 0.30	0.0
(c) $0.5 \leq t' \leq 2.0 \text{ GeV}^2$.			
Events ^a	859		
$K^*(1420)$ events ^a	206 ± 43		
ϵ_D^2	0.24 ± 0.05	$H_D(40)$	0.0 ± 0.08
ϵ_P^2	0.21 ± 0.08	$H_D(41)$	-0.05 ± 0.05
$H_P(20)$	0.19 ± 0.03	$H_D(42)$	0.01 ± 0.03
$H_P(21)$	-0.20 ± 0.09	$H_D(43)$	-0.05 ± 0.04
$H_P(22)$	0.09 ± 0.03	$H_D(44)$	0.01 ± 0.02
	Minimum	Maximum	No interference
$H_D(20)$	0.02 ± 0.04	0.20 ± 0.02	0.38 ± 0.05
r_0	1.0	0.39 ± 0.22	0.0
α_0	4.53 ± 0.16	4.38 ± 0.31	0.0
$H_D(21)$	-0.47 ± 0.07	0.31 ± 0.04	-0.13 ± 0.04
r_1	1.0	1.0	0.0
α_1	4.51 ± 0.09	1.71 ± 0.09	0.0
$H_D(22)$	-0.37 ± 0.03	0.34 ± 0.03	-0.01 ± 0.03
r_2	1.0	1.0	0.0
α_2	4.61 ± 0.10	1.75 ± 0.10	0.0

^a Events in the region $1.1 \leq w(K^-\pi^+) \leq 1.7 \text{ GeV}$.^b To determine this moment, we have set $r_2 = 0$, since $\rho_{22} \approx 0$. (See text for further discussion.)

wave and leads to bigger experimental ranges for $H_D(2M)$.

In Figs. 10–12 are plotted those unnormalized even moments with significant deviation from zero anywhere in the $w(K^-\pi^+)$ region between 1.1 and 1.7 GeV, and the results of the fits are shown as solid curves in these figures. The fitted values for ϵ_P^2 , ϵ_D^2 , $H_P(2M)$, $H_D(LM)$, r_M , and α_M are given in Tables II(a), II(b), and II(c). The solid (dotted) lines in the mass spectra represent the fitted background (P -wave) shape. It can be seen that the fitted curves describe well the experimental moments. The $NH(40)$ moment for the third t' interval [Fig. 12(d)] shows a break near the $K^*(1420)$ mass, and the best fit in this case turns out to be $H_D(40)=0$; the large error quoted for this value [see Table II(c)] reflects a poor fit to this moment.

The most prominent experimental feature is clearly the $NH(20)$ moments for all t' intervals. They peak at the $K^*(1420)$ mass and have the Breit-Wigner shape. What the present analysis shows is that the peaks are “too big” for the number of $K^*(1420)$ events found in the mass spectra and that a considerable amount of S - D interference effects is necessary in order to obtain physical values

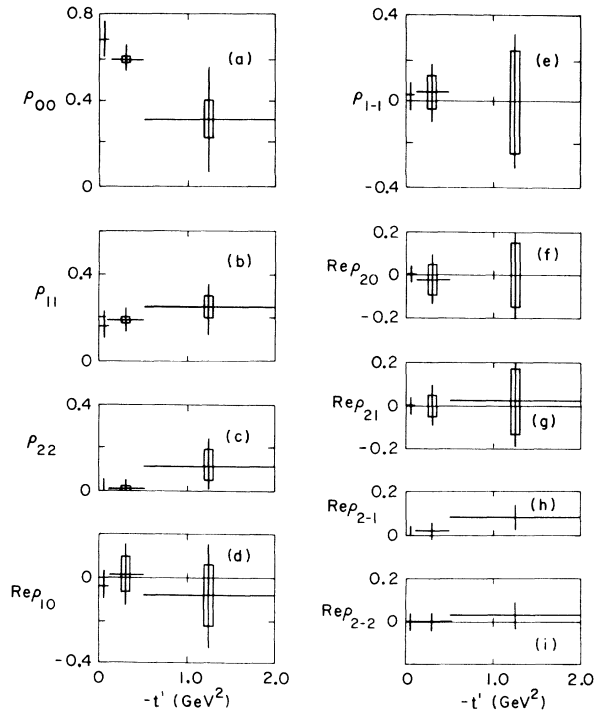


FIG. 13. (a)–(i) $K^*(1420)$ density-matrix elements in the Jackson frame as a function of momentum transfer squared ($-t'$). The vertical bars represent the experimentally allowed ranges.

for the density-matrix elements.

In this connection it is of particular importance to note that for the first t' interval ($|t'| < 0.1$ GeV²) the minimum amount of interference necessary to satisfy the positivity conditions (i.e., $\rho_{22}^{(D)}=0$) approaches the maximum allowable interference (i.e., $r_0 \approx 100\%$). This means that for this case one is able to determine uniquely all the elements of the $K^*(1420)$ density matrix, the first obvious one being that $\rho_{22}^{(D)}=0$. The fact that $\rho_{22}^{(D)}=0$ implies that, as shown in Appendix A, all $\rho_{mm'}^{(D)}=0$ if m or m' is equal to 2. In particular, $\text{Re}\rho_{21}^{(D)}$ and $\text{Re}\rho_{20}^{(D)}$ are both zero, so that $H_D(21)$ and $H_D(22)$ are now proportional to $H_D(41)$ and $H_D(42)$ [see (B5)] which can be determined uniquely from the experimental data.

That $\rho_{22}^{(D)}$ is equal to zero has further implications: It implies that the interference moment $H_{DS}(22)$ should be identically zero [see Eq. (16)] and that $H_{DS}(21)$ is proportional to $\rho_{10}^{(D)}$ [see Eq. (B14)]:

$$H_{DS}(21) = \frac{e^{i\alpha_0}}{[5\rho_{00}^{(D)}]^{1/2}} \rho_{10}^{(D)}. \quad (29)$$

This relation shows that one can determine in this case not only the real part of $\rho_{10}^{(D)}$ but the imaginary part as well. Therefore, with the assumptions of the maximum S - D interference, every single element (real as well as imaginary parts) of the $K^*(1420)$ density matrix can be determined.

In Table III(a) are given two sets of density-matrix elements for the first t' interval: one with the maximum S - D interference and the other with zero interference. Again, we note that without the interference term the value of $\rho_{22}^{(D)}$ is negative by many standard deviations. With $\rho_{22}^{(D)}=0$, the spin-2 positivity conditions reduce to the spin-1 conditions; it can be easily checked that the quoted density-matrix elements satisfy these conditions.

Inspection of Tables II(b) and II(c) shows that the amount of interference required to achieve $\rho_{22}^{(D)}=0$ is less than 100% for the next two t' intervals. We give in Tables III(b) and III(c) the ranges for the density-matrix elements for which it is possible to satisfy the spin-2 positivity conditions. Note that the elements $\text{Re}\rho_{2-1}$ and ρ_{2-2} have unique values, since they are proportional to $H_D(43)$ and $H_D(44)$, which were determined uniquely in this analysis.

We display in Fig. 13 the elements of the $K^*(1420)$ density matrix as a function of t' . We see that the elements $\rho_{mm'}^{(D)}$, for which either m or m' is 2, are consistent with zero, whereas the element $\rho_{00}^{(D)}$ is large, especially in the low t' regions. This observation suggests that the π -exchange contribution is important for the $K^*(1420)$ production

TABLE III. $K^{*0}(1420)$ density-matrix elements (Jackson frame) for three regions of $|t'|$.

(a) $ t' \leq 0.1 \text{ GeV}^2$.		
	Maximum interference	No interference
ρ_{22}	0.0 ± 0.05	-0.34 ± 0.05
ρ_{11}	0.16 ± 0.06	0.32 ± 0.06
ρ_{00}	0.68 ± 0.07	1.03 ± 0.07
$\text{Re}\rho_{10}$	-0.04 ± 0.06	-0.05 ± 0.06
$\text{Im}\rho_{10}$	0.0 ± 0.05	...
ρ_{1-1}	0.03 ± 0.06	0.02 ± 0.06
$\text{Re}\rho_{20}$	0.0 ± 0.03^a	-0.01 ± 0.03
$\text{Re}\rho_{21}$	0.0 ± 0.04^a	-0.04 ± 0.04
$\text{Re}\rho_{2-1}$	0.0 ± 0.03^a	0.0 ± 0.03
ρ_{2-2}	0.0 ± 0.04	0.0 ± 0.04

(b) $0.1 \leq t' \leq 0.5 \text{ GeV}^2$.		
0.0	\leq	$\rho_{22} \leq 0.03 \pm 0.01$
0.19 ± 0.02	\leq	$\rho_{11} \leq 0.20 \pm 0.02$
0.58 ± 0.03	\leq	$\rho_{00} \leq 0.60 \pm 0.03$
-0.07 ± 0.02	\leq	$\text{Re}\rho_{10} \leq 0.10 \pm 0.02$
-0.04 ± 0.02	\leq	$\rho_{1-1} \leq 0.12 \pm 0.02$
-0.08 ± 0.02	\leq	$\text{Re}\rho_{20} \leq 0.05 \pm 0.02$
-0.05 ± 0.02	\leq	$\text{Re}\rho_{21} \leq 0.05 \pm 0.02$
		$\text{Re}\rho_{2-1} = 0.02 \pm 0.02$
		$\rho_{2-2} = 0.0 \pm 0.02$

(c) $0.5 \leq t' \leq 2.0 \text{ GeV}^2$.		
0.05 ± 0.05	\leq	$\rho_{22} \leq 0.19 \pm 0.04$
0.21 ± 0.09	\leq	$\rho_{11} \leq 0.30 \pm 0.05$
0.22 ± 0.15	\leq	$\rho_{00} \leq 0.40 \pm 0.17$
-0.23 ± 0.10	\leq	$\text{Re}\rho_{10} \leq 0.06 \pm 0.09$
-0.24 ± 0.07	\leq	$\rho_{1-1} \leq 0.24 \pm 0.07$
-0.15 ± 0.05	\leq	$\text{Re}\rho_{20} \leq 0.15 \pm 0.05$
-0.13 ± 0.09	\leq	$\text{Re}\rho_{21} \leq 0.17 \pm 0.06$
		$\text{Re}\rho_{2-1} = 0.08 \pm 0.06$
		$\rho_{2-2} = 0.02 \pm 0.06$

^aBecause $\rho_{22}=0$, the imaginary part of this density-matrix element should be zero as well.

in our data. The π -exchange process is also a natural candidate for the S -wave production. That both the S and D waves result from the same production mechanism may explain why the two waves are so strongly coherent.

VI. CONCLUSIONS

In this paper we have shown how to analyze the decay of a resonance into two pseudoscalar mesons in the presence of background interference. For this purpose, we have introduced the concept of interference moments, which may be viewed as a generalization of the familiar multipole moments describing the resonance decays.¹³ From the study of the symmetry relations for these interference moments, we have shown that the interference of

S -wave background with a spin-1 resonance may be ignored by considering the symmetrized angular distributions. On the other hand, the interference of a spin-2 resonance with S -wave background is inseparable from the angular distributions of the resonance alone, so that inclusion in the analysis of the interference effect is essential for the determination of the density-matrix elements.

The fundamental assumption we have made in our analysis is that the background partial waves have smooth mass dependence through the resonance region. This enables us to write down the mass-dependent angular distributions, from which we extract the resonance moments. For the case of the spin-2 resonance, however, we have found that certain moments have contributions not only from the resonance but also from the S - D interference effect whose mass dependence appears very much like the $K^*(1420)$ Breit-Wigner shape. Because of this, we are led to determine only the lower and upper limits for some of the resonance moments.

For the $K^{*0}(890)$ analysis, we have assumed that the P -wave resonance rides on an S -wave background whose mass dependence is linear in the mass region between 0.7 and 1.1 GeV. A system consisting of S and P waves is a relatively simple one. We have, therefore, determined not only the resonance moments but also the interference moments.

For the $K^{*0}(1420)$ analysis, we have assumed that the mass region between 1.1 and 1.7 GeV consists of a D -wave resonance and S - and P -wave backgrounds with the P wave having linear mass dependence. With the data properly symmetrized, it is necessary to consider only the even moments. This means that, of the interference moments, only the S - D interference terms need be considered, and one may ignore the S - P and P - D interference terms.¹⁴ We find that, when the data are so analyzed, the interference effect between the spin-2 state $|20\rangle$ and the S -wave background is so strong that it nearly reaches its maximum allowable value in the small t' region ($|t'| \leq 0.1 \text{ GeV}^2$). This situation can arise only if the production amplitude of the $K^*(1420)$ in the state $|20\rangle$ is the same, except for a proportionality constant, as that of the S -wave background for each combination of the initial and final nucleon helicities. A simple explanation for this may be that the same production mechanism is involved in both the D -wave resonance and the S -wave background. Coupled with the observation that the density-matrix element $\rho_{00}^{(D)}$ is large for small t' regions, the π -exchange mechanism seems a natural candidate for producing the strong interference effect.

There has been some interest as to whether there exist daughter states under the $K^*(890)$ or

$K^*(1420)$ resonances. What the present analysis shows is that S -wave daughter states are *not* required to obtain a good description of our data. This does not mean, however, that daughter states cannot exist in our data. This question can only be answered from a full $K\pi$ phase-shift analysis, a field altogether different from that to which we address ourselves here. We feel that the current theoretical understanding of exchange processes, including absorptive effects, is not reliable enough for us to perform a meaningful $K\pi$ phase-shift analysis.

Firestone *et al.*¹⁵ have claimed evidence for the existence of an S -wave resonance of slightly different mass near the $K^*(1420)$ peak. Their conclusions have been arrived at by examining the mass spectra with different cuts on the Jackson angular distribution. We point out that the identical angular-distribution cuts on our data do not show a shift in the value of the $K^*(1420)$ mass, in contrast to the observations of Firestone *et al.*¹⁵ Translated into our language, this is due to the fact that the interference phase α_0 is near $\pm\pi/2$ in our data. However, it is easy to see that, if α_{μ} is different from $\pm\pi/2$, the S - D interference effect can cause a considerable shift in the resonance peak if the angular cut is made. We therefore conclude that it is not possible to ascertain existence of a nearby resonance by making cuts on the decay angular distribution of a resonance.

ACKNOWLEDGMENTS

The support and encouragement of Dr. N. P. Samios are deeply appreciated. We acknowledge the help of Dr. J. B. Kinson in many stages of this experiment. We thank the AGS and 80-inch-bubble-chamber staffs and crews for their help in obtaining the pictures and our data-handling personnel for their efforts.

APPENDIX A

We present here the definition of the generalized density matrix in terms of the production amplitudes and exhibit the inequalities that have to be satisfied by the density-matrix elements. In addition, we give explicitly the spin-1 and spin-2 positivity conditions for density matrices evaluated in the Jackson frame (or in any frame with z axis in the production plane).

Let $A_{m\mu}^{(i)}$ be the production amplitude for a particle of spin s_i in the state $|s_i m\rangle$ and let μ stand for all other spin indices that are necessary to fully specify the amplitude, e.g., the initial and the final nucleon helicities in reaction (1). Then, the

generalized density-matrix elements for spins s_i and s_j may be written

$$\rho_{mm'}^{(ij)} = \sum_{\mu} A_{m\mu}^{(i)} A_{m'\mu}^{(j)*} . \quad (\text{A1})$$

If the two particles represented by spins s_i and s_j are different, (A1) measures the interference between the states $|s_i m\rangle$ and $|s_j m'\rangle$, whereas if the two particles are identical, it reduces to the definition of the familiar trace-one Hermitian density-matrix element for spin s_i .¹⁶ The generalized Hermiticity takes the form, from this definition,

$$\rho_{mm'}^{(ij)} = \rho_{m'm}^{(ji)*} . \quad (\text{A2})$$

It is easy to show by considering a reflection through the production plane¹³ that, if parity is conserved in the production process, the density-matrix elements (A1) satisfy, in addition,

$$\rho_{-m-m'}^{(ij)} = \eta_i \eta_j (-)^{s_i - s_j} (-)^{m - m'} \rho_{mm'}^{(ij)} , \quad (\text{A3})$$

where η_i (η_j) stands for the intrinsic parity of the particle with spin s_i (s_j). Note that if the two particles are identical, (A3) reduces to the familiar symmetry relation for ordinary density-matrix elements.

We now derive an important inequality for the density-matrix elements (A1) which limits the size of the interference density-matrix elements. Note that the right-hand side of (A1) may be considered a scalar product of two complex vectors; by applying the Schwarz inequality, one then obtains

$$|\rho_{mm'}^{(ij)}|^2 \leq \rho_{mm}^{(ii)} \rho_{m'm'}^{(jj)} . \quad (\text{A4})$$

This shows that the interference density-matrix elements are bounded by the diagonal density-matrix elements of the particles s_i and s_j . The inequality (A4) applies as well to the ordinary density-matrix elements, i.e., to the case $i=j$. In this case, the inequality implies that the off-diagonal density-matrix elements have upper bounds given by the diagonal elements:

$$|\rho_{mm'}^{(ii)}|^2 \leq \rho_{mm}^{(ii)} \rho_{m'm'}^{(ii)} . \quad (\text{A5})$$

It should be noted, however, that the full positivity conditions give in general more stringent conditions than those provided by (A5), with one exception: From (A3) and (A5) for $m' = -m$, one obtains

$$|\rho_{m-m}^{(ii)}| \leq \rho_{mm}^{(ii)} . \quad (\text{A6})$$

It will be shown below that (A6) forms a part of the set of positivity conditions for spin-1 and spin-2 density matrices.

Let us now turn to a discussion of the positivity conditions. Ordinary density-matrix elements are Hermitian, so that the density matrix can be diagonalized by a unitary transformation. The positivity conditions result from the fact that the proba-

bilistic nature of the density matrix demands that its eigenvalues be non-negative. The general prescription^{17,18} for deriving the positivity conditions is well known; one solves for the eigenvalues of the density matrix and requires that they be non-negative.

Owing to parity conservation in the production process, not all elements of the density matrix are independent, and the characteristic polynomial becomes a product of two polynomials. Thus, for the case of the spin-1 density matrix, the characteristic polynomial of order three breaks up into two polynomials of order one and two. Similarly, the fifth-order characteristic polynomial of spin 2 becomes a product of second- and third-order polynomials.

Our aim here is not so much to give a general treatment of the positivity conditions as to exhibit clearly the spin-2 positivity conditions evaluated in the Jackson frame. To this end, we first treat the case of the spin-1 density matrix, since that of spin 2 can be handled in the same fashion, albeit with more complex algebra.

1. Spin-1 Density Matrix

Let us first start with the spin-1 density matrix evaluated in the Jackson frame:

$$\rho = \begin{bmatrix} \rho_{11} & \rho_{10} & \rho_{1-1} \\ \rho_{10}^* & \rho_{00} & -\rho_{10}^* \\ \rho_{1-1} & -\rho_{10} & \rho_{11} \end{bmatrix}.$$

By suitable adjustments of the rows and columns the characteristic polynomial

$$\Delta(\lambda) \equiv \det(\lambda I - \rho) = 0 \quad (\text{A7})$$

can be factorized into two polynomials as follows:

$$\lambda - a = 0, \quad (\text{A8})$$

$$\begin{vmatrix} \lambda - e & p^*/\sqrt{2} \\ \sqrt{2}p & \lambda - b \end{vmatrix} = 0, \quad (\text{A9})$$

where λ stands for the eigenvalue and

$$\begin{aligned} a &= \rho_{11} + \rho_{1-1}, \\ b &= \rho_{11} - \rho_{1-1}, \\ e &= \rho_{00}, \\ p &= \sqrt{2}\rho_{10}. \end{aligned} \quad (\text{A10})$$

If we write a polynomial of order n in λ as

$$\Delta(\lambda) = \sum_{k=0}^n (-)^k f_k \lambda^{n-k}, \quad f_0 = 1 \quad (\text{A11})$$

the necessary and sufficient condition that the roots are non-negative is

$$f_k \geq 0, \quad k=0, n. \quad (\text{A12})$$

Applying this rule (the Descartes rule of signs¹⁹) to (A8) and (A9), we obtain

$$\begin{aligned} a &\geq 0, \\ b + e &\geq 0, \\ be &\geq |p|^2, \end{aligned} \quad (\text{A13})$$

which may be written succinctly in terms of the density-matrix elements as follows:

$$\begin{aligned} \rho_{11} &\geq |\rho_{1-1}|, \\ \rho_{00}(\rho_{11} - \rho_{1-1}) &\geq 2|\rho_{10}|^2. \end{aligned} \quad (\text{A14})$$

The inequalities (A14) then represent the full positivity conditions for the spin-1 density matrix evaluated in any frame in which the quantization axis lies in the production plane. If a resonance decays into two pseudoscalars, it is not possible to measure the imaginary parts of the density-matrix elements. For the case of a spin-1 resonance, this means that $\text{Im}\rho_{10}$ cannot be measured and the positivity conditions (A14) should be modified by replacing the absolute value of ρ_{10} by its real part. As we shall see, the problem of projecting the positivity conditions into the space of measured variables becomes nontrivial in the case of the spin-2 density matrix.

2. Spin-2 Density Matrix

We start with a spin-2 density matrix evaluated in the Jackson frame and follow the steps outlined in the spin-1 section. The fifth-order characteristic polynomial breaks up into two separate polynomials as follows:

$$\begin{vmatrix} \lambda - d & -u \\ -u^* & \lambda - a \end{vmatrix} = 0, \quad (\text{A15})$$

$$\begin{vmatrix} \lambda - e & p^*/\sqrt{2} & -q^*/\sqrt{2} \\ \sqrt{2}p & \lambda - b & v^* \\ -\sqrt{2}q & v & \lambda - c \end{vmatrix} = 0, \quad (\text{A16})$$

where

$$\begin{aligned} a &= \rho_{11} + \rho_{1-1}, & b &= \rho_{11} - \rho_{1-1}, \\ c &= \rho_{22} + \rho_{2-2}, & d &= \rho_{22} - \rho_{2-2}, \\ u &= \rho_{21} + \rho_{2-1}, & v &= \rho_{21} - \rho_{2-1}, \\ e &= \rho_{00}, & p &= \sqrt{2}\rho_{10}, & q &= \sqrt{2}\rho_{20}. \end{aligned} \quad (\text{A17})$$

Note that p , q , u , and v are in general complex, while all other variables are real.

Applying the Descartes rule of signs to the polynomials (A15) and (A16) and separating out the unmeasured from the measured variables, one ob-

tains for the spin-2 positivity conditions

$$f_1 \geq 0, \quad f_2 \geq \Phi_1, \quad f_3 \geq 0, \quad f_4 \geq \Phi_2, \quad f_5 \geq \Phi_3, \quad (\text{A18})$$

where

$$\begin{aligned} f_1 &= a + d, \\ f_2 &= ad - u_R^2, \\ f_3 &= b + c + e, \\ f_4 &= be - p_R^2 + c(b + e) - q_R^2 - v_R^2, \\ f_5 &= c(be - p_R^2) - bq_R^2 - ev_R^2 + 2p_R q_R v_R, \\ \Phi_1 &= u_I^2, \\ \Phi_2 &= p_I^2 + q_I^2 + v_I^2, \\ \Phi_3 &= cp_I^2 + bq_I^2 + ev_I^2 - 2v_R p_I q_I \\ &\quad - 2p_R q_I v_I + 2q_R p_I v_I. \end{aligned} \quad (\text{A19})$$

Here subscripts R and I denote the real and imaginary parts.

We see that f_1 to f_5 are measurable, whereas Φ_1 , Φ_2 , and Φ_3 involve unmeasured variables. However, the minima of these functions can be calculated to give

$$\begin{aligned} \Phi_1|_{\min} &= \Phi_2|_{\min} = 0, \\ \Phi_3|_{\min} &= \mu f_4, \\ \mu &= \min\{0, \chi_1, \chi_2, \chi_3\}, \end{aligned} \quad (\text{A20})$$

where χ_1 , χ_2 , and χ_3 are the three roots of the equation

$$\chi^3 - f_3 \chi^2 + f_4 \chi - f_5 = 0. \quad (\text{A21})$$

Combining (A20) with (A18), one obtains a set of constraints on the measured parts of the spin-2 density-matrix elements, which result from the positivity conditions. This is the form given in the paper by Bassompierre *et al.*²

However, one can go further than this. Note first that (A18) and (A20) imply that f_3 and f_4 have to be positive. If f_5 is negative, it can be shown that μ is also negative, but its value is such that

$$f_5 < \Phi_3|_{\min},$$

in contradiction to the Eqs. (A18). From this argument, one sees that the full positivity conditions impose on the measured variables the following constraints¹⁸:

$$f_i \geq 0, \quad i = 1, 5 \quad (\text{A22})$$

which can be rearranged to give the following set of inequalities:

$$\rho_{11} \geq |\rho_{1-1}|, \quad (\text{A23})$$

$$be \geq p_R^2, \quad (\text{A24})$$

$$\rho_{22} \geq |\rho_{2-2}|, \quad (\text{A25})$$

$$ad \geq u_R^2, \quad (\text{A26})$$

$$be - p_R^2 + c(b + e) \geq q_R^2 + v_R^2, \quad (\text{A27})$$

$$c(be - p_R^2) \geq bq_R^2 + ev_R^2 - 2p_R q_R v_R. \quad (\text{A28})$$

The inequality (A24) is a consequence of (A27) and (A28); however, it is convenient to include it in the full set of positivity conditions. Note that the first three conditions imply that diagonal elements ρ_{00} , ρ_{11} , and ρ_{22} are all positive (or zero). Note also that the first two inequalities are identical in form to the positivity conditions of the spin-1 density matrix [see (A14)]. It can be shown that, as a consequence of (A24), the inequalities (A27) and (A28) restrict the variables q_R and v_R to lie within a circle and an ellipse, respectively, and that the major axis of the ellipse is smaller than the radius of the circle. These observations imply that the inequality (A27) is in general redundant. However, if $be = p_R^2$, then (A28) implies that q_R and v_R form a line, while (A27) restricts the line to within a circle. Of course, the mathematical equality $be = p_R^2$ never happens in reality, and so the inequality (A27) may be considered redundant for all practical purposes.

Suppose now that $\rho_{22} = 0$. We will see that this imposes a severe constraint on the other density-matrix elements due to the positivity conditions. From (A25), we see that $\rho_{2-2} = 0$ in this case, so that $c = d = 0$ [see (A17)]. This in turn implies that $u_R = 0$ from (A26). It can be shown that, if $c = 0$, (A27) and (A28) can be satisfied simultaneously only if $q_R = v_R = 0$. From this we can conclude that, if $\rho_{22} = 0$, the positivity conditions cannot be satisfied unless $\rho_{mm'} = 0$ if m or $m' = 2$. This statement applies to the imaginary as well as to the real part of $\rho_{mm'}$, since the derivation outlined here can be applied as well to the full complex density-matrix elements. We note that this conclusion can be derived trivially, if we go back to the definition (A1) of the density-matrix elements. If $\rho_{mm}^{(ii)} = 0$ for a given m , Eq. (A1) shows that the corresponding amplitude $A_{m\mu}^{(ii)}$ itself should be zero for all μ . Consequently, any density-matrix element containing that particular m as an index must also be zero. What we emphasize here is that this fact is naturally contained in the set of positivity conditions given in (A23) to (A28).

APPENDIX B

It is the main purpose of this Appendix to exhibit explicitly the relationship between the moments and the density-matrix elements for spins 1 and 2. Our starting point is Eq. (10), which can be inverted to yield

$$\rho_{mm'}^{(ij)} = \sum_L \frac{2L+1}{(2s_i+1)^{1/2}(2s_j+1)^{1/2}} \times \frac{(s_j m' LM | s_i m)}{(s_j 0 L 0 | s_i 0)} H_{ij}(LM). \quad (\text{B1})$$

It is convenient to write down two special cases of this relation. Let us consider as a first case the ordinary resonance density matrix, i.e., $s_i = s_j = J$:

$$\text{Re} \rho_{mm'}^{(J)} = \sum_{\text{even } L} \left(\frac{2L+1}{2J+1} \right) \frac{(Jm' LM | Jm)}{(J 0 L 0 | J 0)} H_J(LM). \quad (\text{B2})$$

This relation shows that measurement of even moments gives the real part of the density-matrix elements. A second special case of (B1) is of interest for our purposes. It concerns the case when the spin s_j is zero:

$$\rho_{m0}^{(J0)} = (2J+1)^{1/2} H_{J0}(Jm), \quad (\text{B3})$$

where we have set $s_i = J$. This shows that the interference moment between spin J and spin 0 is proportional to the interference density-matrix element.

We now present explicitly the spin-1 density-matrix elements (denoted by $\rho_{mm'}^{(P)}$) in terms of the spin-1 moments $H_P(LM)$. Using (B2), we obtain

$$\begin{aligned} \rho_{00}^{(P)} &= \frac{1}{3} [1 + 5H_P(20)], \\ \rho_{11}^{(P)} &= \frac{1}{3} [1 - \frac{5}{2}H_P(20)], \\ \text{Re} \rho_{10}^{(P)} &= \frac{5}{2\sqrt{3}} H_P(21), \\ \rho_{1-1}^{(P)} &= -\frac{5}{\sqrt{6}} H_P(22). \end{aligned} \quad (\text{B4})$$

Similarly, the spin-2 density-matrix elements $\rho_{mm'}^{(D)}$ can be given in terms of the moments $H_D(LM)$ as follows:

$$\begin{aligned} \rho_{00}^{(D)} &= \frac{1}{5} [1 + 5H_D(20) + 9H_D(40)], \\ \rho_{11}^{(D)} &= \frac{1}{5} [1 + \frac{5}{2}H_D(20) - 6H_D(40)], \\ \rho_{22}^{(D)} &= \frac{1}{5} [1 - 5H_D(20) + \frac{3}{2}H_D(40)], \\ \text{Re} \rho_{10}^{(D)} &= \frac{1}{2} H_D(21) + 3(\frac{3}{10})^{1/2} H(41), \\ \text{Re} \rho_{21}^{(D)} &= (\frac{3}{2})^{1/2} H_D(21) - \frac{3}{2} (\frac{1}{5})^{1/2} H(41), \\ \text{Re} \rho_{20}^{(D)} &= -H_D(22) + \frac{3}{2} (\frac{3}{5})^{1/2} H_D(42), \\ \rho_{1-1}^{(D)} &= -(\frac{3}{2})^{1/2} H_D(22) - 3(\frac{2}{5})^{1/2} H_D(42), \\ \text{Re} \rho_{2-1}^{(D)} &= -\frac{3}{2} (\frac{7}{5})^{1/2} H_D(43), \\ \rho_{2-2}^{(D)} &= 3(\frac{7}{10})^{1/2} H_D(44). \end{aligned} \quad (\text{B5})$$

Let us now come back to a discussion of the interference density matrix between the spins J and

0 [see (B3)]. The relation (A4) in this case assumes the form

$$|\rho_{m0}^{(J0)}|^2 \leq \rho_{mm}^{(J)} \quad (\text{B6})$$

so that it is convenient to parametrize the interference density matrix as follows:

$$\rho_{m0}^{(J0)} = [\rho_{mm}^{(J)}]^{1/2} r_m e^{i\alpha_m}, \quad (\text{B7})$$

where $0 \leq r_m \leq 1$ and $0 \leq \alpha_m \leq 2\pi$. Combining this with (B3), we obtain for the interference moments

$$H_{J0}(Jm) = \left(\frac{\rho_{mm}^{(J)}}{2J+1} \right)^{1/2} r_m e^{i\alpha_m}. \quad (\text{B8})$$

This is the form we have used to parametrize the interference of the S-wave background with the spin-1 and spin-2 resonances in the $K^-\pi^+$ system.

Suppose now that for $m=0$ the parameter r_0 turns out to be equal to 1. From the definition of density matrices (A1), it can be shown that in this case

$$A_{0\mu}^{(J)} = a A_{0\mu}^{(0)}, \quad (\text{B9})$$

where a is in general complex and independent of the index μ . The relevant density-matrix elements then have the form

$$\begin{aligned} \rho_{00}^{(0)} &= \sum_{\mu} |A_{0\mu}^{(0)}|^2 = 1, \\ \rho_{00}^{(J)} &= \sum_{\mu} |A_{0\mu}^{(J)}|^2 = |a|^2 \sum_{\mu} |A_{0\mu}^{(0)}|^2 = |a|^2, \\ \rho_{00}^{(J0)} &= \sum_{\mu} A_{0\mu}^{(J)} A_{0\mu}^{(0)*} = a \sum_{\mu} |A_{0\mu}^{(0)}|^2 = a. \end{aligned} \quad (\text{B10})$$

On the other hand, from (B7) we obtain

$$\rho_{00}^{(J0)} = [\rho_{00}^{(J)}]^{1/2} e^{i\alpha_0} \quad (\text{B11})$$

so that

$$A_{0\mu}^{(J)} = [\rho_{00}^{(J)}]^{1/2} e^{i\alpha_0} A_{0\mu}^{(0)}. \quad (\text{B12})$$

Using this formula, the interference density matrix can be written

$$\begin{aligned} \rho_{m0}^{(J0)} &= \sum_{\mu} A_{m\mu}^{(J)} A_{0\mu}^{(0)*} \\ &= [\rho_{00}^{(J)}]^{-1/2} e^{i\alpha_0} \rho_{m0}^{(J)} \end{aligned} \quad (\text{B13})$$

or

$$H_{J0}(Jm) = \frac{e^{i\alpha_0} \rho_{m0}^{(J)}}{[(2J+1)\rho_{00}^{(J)}]^{1/2}}. \quad (\text{B14})$$

This shows explicitly that, if $r_0 = 1$, the measurement of the interference moment yields the real as well as the imaginary part of $\rho_{m0}^{(J)}$.²⁰

*Work supported by the U. S. Atomic Energy Commission.

¹M. Aguilar-Benitez, R. L. Eisner, and J. B. Kinson, Phys. Rev. D 4, 2583 (1971).

²Additional references in which $K^*(1420)$ density-matrix elements are given: Y. W. Kang, Phys. Rev. 176, 1587 (1968); G. Bassompierre *et al.*, Nucl. Phys. B13, 189 (1969); M. Deutschmann *et al.*, Aachen-Berlin-CERN-London-Vienna Collaboration, *ibid.* B36, 373 (1972).

³References in which $f^0(1260)$ density-matrix elements can be found: F. Crijns *et al.*, Aachen-Berlin-CERN Collaboration, Phys. Letters 22, 533 (1966); H. Cohn *et al.*, Nucl. Phys. 82, 690 (1966); J. Poirier *et al.*, Phys. Rev. 163, 1462 (1967); R. L. Eisner *et al.*, *ibid.* 164, 1699 (1967).

⁴In the $K^-\pi^+$ rest frame, we use the K^- direction as the analyzer with the z axis chosen along the incident beam direction and the y axis along the production normal.

⁵We use the shorthand notation $D_{mm'}^l(\Omega) = D_{mm'}^l(\varphi, \theta, 0)$.

⁶M. E. Rose, *Elementary Theory of Angular Momentum* (Wiley, New York, 1957).

⁷S. M. Berman and M. Jacob, Phys. Rev. 139, B1023 (1965).

⁸D. H. Miller *et al.*, Phys. Rev. 153, 1423 (1967). The generalized density-matrix elements $\rho_{mm'}^{ij}$, given in this reference correspond to $\epsilon_i \epsilon_j \rho_{mm'}^{ij}$ in our notation.

⁹We have used the CERN minimization program MINUIT.

¹⁰In fact, the one-pion-exchange model with absorption gives a good description of the data: M. Aguilar-Benitez *et al.*, Phys. Rev. Letters 26, 466 (1971).

¹¹Note that it is not necessary to symmetrize the data in a maximum-likelihood analysis, for the theoretical formula we use already has the symmetry built in. However, the symmetrized data have to be used when the fit is compared with the data.

¹²With zero S - D interference term, we obtain ρ_{22}

$= -0.26 \pm 0.04$ for $0.1 < -t' < 0.5$ GeV² and $\rho_{22} = -0.18 \pm 0.06$ for $0.5 < -t' < 2.0$ GeV².

¹³The resonance moments $H_{ii}(LM)$ are proportional to the well-known multipole parameters: See S. U. Chung, CERN Yellow Report No. CERN 71-8, 1971; Phys. Rev. 169, 1342 (1968).

¹⁴For completeness, we have also fitted the odd interference moments $H(1M)$ and $H(3M)$ by using the full distribution function, with acceptable fits in the entire mass range $w(K^-\pi^+) < 1.6$ GeV; however, examination of odd moments for $w(K^-\pi^+)$ above 1.6 GeV indicates that a non-negligible amount of D wave (or higher waves) not associated with the $K^*(1420)$ resonance might be required to give a good description of the data.

¹⁵A. Firestone, G. Goldhaber, and D. Lissauer, Phys. Rev. Letters 26, 1460 (1971).

¹⁶The production amplitude has been normalized such that $\text{tr}\{\rho^{ii}\} = 1$.

¹⁷P. Minnaert, Phys. Rev. 151, 1306 (1966).

¹⁸R. H. Dalitz, Nucl. Phys. 87, 89 (1966); M. G. Doncel, L. Michel, and P. Minnaert, Laboratoire de Physique Théorique (Université de Bordeaux, 33-Talence, France), Reports No. PTB-35, No. PTB-37, and No. PTB-41 (unpublished). See these references for the spin-2 positivity conditions for the density-matrix elements evaluated in the transversity frame.

¹⁹C. V. Durell and A. Robson, *Advanced Algebra* (Bell, London, 1937), p. 287.

²⁰We wish to point out that the condition $r_0 = 1$ and its consequences (B11) and (B13) do not violate the generalized positivity conditions which include the interference density-matrix elements. The value of r_m for $m \neq 0$, on the other hand, may not in some cases attain its maximum due to the positivity conditions. However, none of the results presented in this paper are significantly affected by this constraint. The generalized positivity conditions involving the interference density-matrix elements will be dealt with in detail in a future publication.